**Atmospheric
Chemistry
and Physics
Discussions**

# Parametric representation of the cloud droplet spectra for LES warm bulk microphysical schemes

**O. Geoffroy[1], J.-L. Brenguier[2], and F. Burnet[2]**

[1]Royal Netherlands Meteorological Institute (KNMI), De Bilt, The Netherlands
[2]GAME/CNRM (Météo-France, CNRS), Toulouse, France

17633

## Abstract

Parametric functions are currently used to represent droplet spectra in clouds and to develop bulk parameterizations of the microphysical processes and of their interactions with radiation. The most frequently used parametric functions are the Lognormal and the Generalized Gamma which have three and four independent parameters, respectively. In a bulk parameterization, two parameters are constrained by the total droplet number concentration and the liquid water content. In the Generalized Gamma function, one parameter is specified a priori, and the fourth one, like the third parameter of the Lognormal function, shall be tuned, for the parametric function to statistically best fit observed droplet spectra.

These parametric functions are evaluated here using droplet spectra collected in non-or slightly precipitating stratocumulus and shallow cumulus. Optimum values of the tuning parameters are derived by minimizing either the absolute or the relative error for successively the first, second, fifth, and sixth moments of the droplet size distribution. A trade-off value is also proposed that minimizes both absolute and relative errors for the four moments concomitantly. Finally, a parameterization is proposed in which the tuning parameter depends on the liquid water content. This approach significantly improves the fit for the smallest and largest values of the moments.

## 1 Introduction

Cloud particles are represented by their size distribution also referred to as spectrum. In the liquid phase, the spectrum originates from activation of cloud condensation nuclei (CCN), mainly at cloud base. Hence it expends from submicron particles for the smallest activated CCNs to about $10\,\mu$m in radius for the giant ones. As particles grow by condensation, the spectrum gets narrower because the growth rate of a droplet is inversely proportional to its size. Higher in a cloud, spectral narrowing is counterbalanced by broadening processes, mainly by turbulent mixing, because particles

17634

experience different growth histories along different trajectories, some ascending adiabatically from cloud base, while others undergo dilution with environmental air and partial evaporation. New CCNs can also be activated higher than cloud base, when moist and clear air is entrained in an updraft, hence initiating small droplets. When the biggest droplets reach a radius of about $20\,\mu$m, collision and coalescence generate drizzle particles (from 20 to a few $100\,\mu$m). If the cloud is sufficiently deep and the liquid water content large enough, droplets and drops continue to collide to form precipitation drops (mm). The maximum drop radius, of the order of $4\,$mm, is limited by break-up, either following a collision or spontaneously for the biggest drops. The total number concentration spans over a large range, because millions of droplets are necessary to form a drop. It thus evolves from up to $1000\,$cm$^{-3}$ for droplets in a polluted environment, to a few per cubic meter for precipitation drops. Because the number concentration of activated CCN, the convective cell trajectories, the series of mixing events and the resulting growth histories by condensation, collection and break-up are infinitely diverse, cloud particle spectra exhibit all kinds of shapes (Warner, 1969a, b, 1970, 1973a, b).

The cloud droplet size distribution (CDSD) is expressed as a concentration density, $n(r)dr$, i.e. number density of droplets per volume (or per mass) of air, and per unit size. To summarize the properties of a size distribution, one commonly uses a moment of the distribution $M_p$, or the mean radius of the $p^{th}$ moment $r_p$:

$$M_p = \int_0^\infty r^p n(r)dr, \tag{1}$$

$$r_p = \left( M_p / N \right)^{\frac{1}{p}} \tag{2}$$

where $N = M_0$ is the total number concentration.

To interpret microphysical observations, examine the interactions between cloud microphysics and other physical processes, and numerically simulate these interactions,

parametric functions are frequently used to reduce the variety of the droplet spectral shapes. The objective in this paper is to evaluate parametric functions that best replicate observed spectra on a statistical basis. The focus is on non-or slightly precipitating stratocumulus and shallow cumulus clouds.

After a brief description (Sect. 2) of bulk microphysics schemes, three frequently used parametric functions are described in Sect. 3. The methodology for tuning the functions and the data sets on which tuning relies are detailed in Sects. 4 and 5, respectively. Section 6 addresses the specific issue of scaling up small scale measurements for characterizing cloud system properties. The results are then reported in Sect. 7, for fixed and variables values of the tuning parameters successively, before the conclusions.

## 2  Bulk parameterizations and parametric functions

In a numerical model, the natural variability of the droplet spectra can be explicitly simulated with "bin" microphysical schemes where the number distribution is discretized, from 30 to 200 size classes (Kogan, 1991). The computational cost of such schemes however, prevents their use in large domain, high spatial resolution, cloud resolving models. Instead, bulk parameterizations have been developed. Indeed, even though spectra are diverse, one usually observe a transition from droplets to drops, in the size range where condensational growth becomes inefficient, while collection starts to become significant, namely between 20 and $50\,\mu$m in radius. This size range also corresponds to a rapid increase of the particle fall velocity with the particle radius ($\propto r^2$). In a liquid phase bulk scheme, hydrometeors are thus distributed in two categories, the droplets that do not or slowly sediment, and the drops that precipitate more rapidly. This necessarily introduces errors and biases. The art in the development of bulk parameterizations is therefore to carefully select the minimum number of well suited prognostic variables and develop equations that reflect the physical processes responsible for the evolution of these variables, while minimizing errors and biases.

Bulk parameterizations can be classified according to the number of particle categories, the threshold radius value that separates the categories, and the number of independent variables used to describe each category. For the liquid phase, they are currently limited to two hydrometeor categories, droplets and drops, but the threshold radius depends on the application. For simulation of deep clouds, the threshold radius is generally set to about 40–50 $\mu$m (Berry and Reinhardt, 1974; Seifert and Beheng, 2001), while for shallow clouds a lower threshold of 20–25 $\mu$m is preferred (Khairoutdinov and Kogan, 2000). Note that all independent variables of a parameterization are not necessarily prognostic variables in a numerical model. For instance in Seifert and Beheng (2006), using a Gamma distribution to represent the droplet mass spectrum, the parameter $\nu_c$ is set to 1; in Ackerman et al. (2008) using a Lognormal distribution, the parameter $\sigma_g$ is set to 1.5, although a value of 1.2 is recognized to better fit the observations. Original bulk schemes were limited to one prognostic variable per category: the water content, $q_c$ for the droplets and $q_r$ for the drops (or mixing ratio=$q/\rho_a$, where $\rho_a$ is the air density) (Kessler, 1969; Tripoli and Cotton, 1980). More recent schemes rely on 4 prognostic variables, adding to the water contents the total number concentration in each category, $N_c$ and $N_r$ (Ziegler, 1985; Cohard and Pinty, 2000; Khairoutdinov and Kogan, 2000; Seifert and Beheng, 2001). Beyond the total water content and total number concentration of particles in each category, there were a few attempts to introduce more variety by also predicting additional variables such as the reflectivity, as in Milbrandt and Yau (2005). Table 1 summarizes the characteristics of existing bulk parameterizations for the liquid phase, with a focus on the description of the droplet category.

The physical processes that act as sources and sinks for the particle categories shall then be parameterized. The CCN activation process is a source for the droplet category. The collection process (a sink for the droplets and a source for the drops) is parameterized by accounting for the collection between droplets to form drops (auto-conversion), and the collection of droplets by drops to form bigger drops (accretion). In the most sophisticated schemes, the collection between droplets to form bigger

droplets and the collection between drops to form bigger drops (self-collection) are also considered (Ziegler, 1985; Cohard et Pinty, 2000; Seifert and Beheng, 2006). Indeed, these two last processes do not affect the mass of condensed water in each category, but the number concentration, hence the mean size of the particles and their mean fall velocity.

It is also useful to notice that two methodologies were adopted to develop bulk parameterizations. In the empirical approach (Khairoutdinov and Kogan, 2000), numerical simulations of clouds are performed with a bin microphysics scheme. Each grid box, at each time step, is then used as one realisation of the microphysical processes, from which bulk variables ($q_c$, $q_r$, $N_c$, $N_r$) and their evolution rates by CCN activation, auto-conversion, accretion, and precipitation can be calculated. Empirical laws are then derived by minimization over the whole set of realisations. In such a case, the accuracy of the parameterization is limited by the performance of the bin microphysics scheme and the variable space explored by the simulations. Others (Liu and Daum, 2004) follow a more analytical approach in which the particle size distribution in each category is represented by a parametric function. The stochastic collection equation is then analytically resolved to derive a formulation of the auto-conversion and accretion rates. In this case the accuracy of the solution mainly depends on the realism of the chosen parametric function. Note however, that coefficients of some "analytical type" bulk parameterizations are tuned empirically (Seifert and Beheng, 2001, 2006).

Some physical processes in a cloud model require additional information about cloud microphysics, beyond the prognostic number concentration ($N=M_0$) and water content ($\propto M_3$). For instance, CCN activation is often parameterized using a diagnostic of the peak supersaturation, that depends on the first moment of the size distribution $M_1$, also referred to as the droplet integral radius (Twomey, 1959). Radiative transfer calculations in clouds depend on light extinction that is proportional to the second moment $M_2$ of the droplet spectrum (Hansen and Travis, 1974). The sedimentation flux depends on the droplet sizes, through an approximation of their fall velocity. For particles smaller than 30 $\mu$m in radius, the terminal fall velocity verifying roughly the Stokes' law

(Roger and Yau, 1989), the sedimentation flux of particle number is proportional to the second moment, $M_2$, and the sedimentation flux of water content is proportional to the fifth moment, $M_5$. The radar reflectivity in a liquid phase cloud is proportional to $M_6$ (Atlas, 1954). The width of the size distribution $w = 1/M_0 \sqrt{M_0 M_2 - M_1^2}$, or its dispersion $d = N \cdot w / M_1$, have been used to establish relationships between the mean volume and effective radii of the droplet spectrum for radiative transfer calculations (Liu and Daum, 2000). It is therefore not sufficient for a microphysics bulk parameterization to accurately predict the auto-conversion and accretion rates; it must also provide accurate diagnostics of various integral properties of the cloud droplet spectrum, at least for $M_1$, $M_2$, $M_5$, $M_6$.

In summary, bulk parameterizations that are developed following an analytical approach rely on a priori specified parametric functions for the description of the droplet spectra. Moreover, all bulk parameterizations, including those empirically tuned, also require a priori specified parametric functions to establish formal relationships between the prognostic moments of the droplet size distribution ($M_0$ and $M_3$) and those used in the parameterization of each microphysical process.

## 3 Commonly used parametric functions

To represent droplet size distributions, the most frequently used parametric functions are the Lognormal (Clark, 1976; Feingold et Levin, 1986) and the Generalized Gamma (Liu and Hallett, 1998; Cohard et Pinty, 2000). These two functions are convenient because any of their moments can be expressed as a function of the parameters of the distribution. *The Lognormal function*

$$n_c(r) = N \frac{1}{\sqrt{2\pi} r \ln \sigma_g} \exp\left( -\frac{1}{2} \left( \frac{\ln(r/r_g)}{\ln \sigma_g} \right)^2 \right) \tag{3}$$

has 3 independent parameters, the total number concentration $N$, the geometric standard deviation $\sigma_g$, and the mean geometric radius $r_g$, where $r_g = e^{<\ln(r)>}$. The $p^{th}$ moment of the spectrum is directly related to $N$, $\sigma_g$, and $r_g$ via:

$$M_p = N r_g^p \exp\left( \frac{p^2}{2} (\ln \sigma_g)^2 \right), \tag{4}$$

and it is expressed as a function of $N$, $M_3$ and $\sigma_g$ as

$$M_p = N^{1-p/3} M_3^{p/3} \exp\left( \frac{p^2 - 9}{2} \ln(\sigma_g)^2 \right). \tag{5}$$

*The Generalised Gamma function*

$$n(r) = N \frac{\alpha}{\Gamma(v)} \lambda^{\alpha v} r^{\alpha v - 1} \exp(-(\lambda r)^\alpha) \tag{6}$$

has 4 independent parameters, $N$, the slope parameter $\lambda$ and the two shape parameters $\alpha$ and $v$. The $p^{th}$ moment of the spectrum is directly related to $N$, $\lambda$, $\alpha$ and $v$ via:

$$M_p = \frac{N}{\lambda^p} \left( \frac{\Gamma(v + \frac{p}{\alpha})}{\Gamma(v)} \right) \tag{7}$$

and it is expressed as a function of $N$, $M_3$, $\alpha$ and $v$ as:

$$M_p = N^{1-p/3} M_3^{p/3} \frac{\Gamma(v + \frac{p}{\alpha})}{\Gamma(v + \frac{3}{\alpha})^{\frac{p}{3}}} \Gamma(v)^{\frac{p-3}{3}}. \tag{8}$$

The Generalized Gamma function includes the Gamma (or Golovin), the Exponential and the Weibull functions. Indeed, the Gamma function (Liu and Daum, 2004) is a Generalized Gamma with $\alpha = 1$ (hereafter referred to as GG1). Some authors use the

Gamma function to represent the cloud droplet mass distribution (Berry and Reinhardt, 1974; Williams and Wojtowicz, 1982; Seifert and Beheng, 2001), which is equivalent of using a Generalized Gamma function with $\alpha=3$ (hereafter referred to as GG3) for describing the particle number concentration distribution. In this paper, both values, $\alpha=1$ and $\alpha=3$, are evaluated.

In summary, in the framework of a bulk parameterization with two prognostic variables for the droplet category ($M_0$ and $M_3$), there is still one parameter to adjust, hereafter referred to as the tuning parameter, either $\sigma_g$ for the Lognormal or $\nu$ for the Generalised Gamma function, where $\alpha$ has been specified to either 1 or 3.

## 4 Methodology

The objective in this paper is to determine which value of the tuning parameter allow the parametric function to statistically best fit the observed droplet spectra. More specifically we will address the following questions.

– When a Lognormal, a GG1 or a GG3 function is used, and the tuning parameter is constant, what is the best value to use for this parameter?

– Is the accuracy improved if the tuning parameter is allowed to vary?

– In such a case how can it be diagnosed from the two prognostic variables $N$ and $q_c$?

To answer these questions, a large sample of droplet spectra measured in diverse types of non- or slightly precipitating shallow clouds is used. The best fit to each observed spectrum is obtained with either a Lognormal or a Generalized Gamma function that has the same droplet number concentration and liquid water content, and a value of the tuning parameter, $\sigma_g$ for the Lognormal, $\nu_1$ for GG1 and $\nu_3$ for GG3, that minimizes the difference between an integral property of the observed spectrum and the one of the parametric function. The integral properties considered here are $M_1$, $M_2$,

$M_5$, $M_6$. For each one separately, the value of the tuning parameter that minimizes the mean absolute error between the property value of the observed spectrum ($x_m$) and the one derived from the fitted parametric function ($x_p$) is calculated. The same procedure is applied to the relative error, where the absolute $\varepsilon_{abs}$ and relative $\varepsilon_{rel}$ errors are defined as: $\varepsilon_{abs}=x_p-x_m$ and $\varepsilon_{rel}=x_p/x_m$. The statistical adequacy of the tuning parameter value is then evaluated for each moment successively. Since there is no reason for a single value of the tuning parameter to minimize the errors for the 4 moments concomitantly, a trade-of value is also evaluated in terms of absolute and relative errors.

In the second step, a parameterization is proposed to allow the value of the tuning parameter to vary, and the resulting errors, both absolute and relative, are calculated for comparison with the ones obtained in step 1.

## 5 The data sets

Cloud particle size distributions used in this study were collected during two airborne field experiments: The ACE-2 campaign took place in June and July 1997 to document marine boundary layer stratocumulus clouds, north of the Canary islands (Brenguier et al., 2000). The RICO campaign took place in December 2004 and January 2005 to study shallow precipitating cumulus clouds of the coast of the Caribbean Island of Antigua and Barbuda within the Northeast Trades of the western Atlantic (Rauber et al., 2007).

The droplet spectra were measured with the Fast-FSSP, a droplet spectrometer that covers a range from 1 to about 20–25 $\mu$m in radius (Brenguier et al., 1998). The droplet spectra are extended beyond 25 $\mu$m with data from a PMS-OAP-200-X (PMS Inc, Boulder Colorado, USA) during ACE-2 and a PMS-OAP-260-X during RICO. The 200-X measures drizzle particle sizes over 15 radius bins from 7.5 to 155 $\mu$m, with a bin width of 10 $\mu$m. The 260-X covers a larger range, from 2.5 to 317.5 $\mu$m, with 63 bins of 5 $\mu$m width. Cloud droplets are then defined as particles with a radius smaller than 37.5 $\mu$m.

This value is selected because it corresponds to a bin limit in both the OAP-200-X and -260-X and it is intermediate between the values used in most bulk parameterizations. A sensitivity study suggests that the selected threshold radius value has no noticeable impact on the results within the range from 27.5 to 37.5 $\mu$m.

These two campaigns were selected because significant differences were expected between the stratocumulus and the shallow cumulus regimes. The depth of the stratocumulus clouds in ACE-2 was a few hundreds of meters, while it reaches a few kilometres for the RICO shallow cumuli. In ACE-2, the droplet number concentration varied from less than 50 to more than 400 cm$^{-3}$, while it was lower during RICO with values less than 100 cm$^{-3}$ in most cases. Light precipitation was observed in ACE-2, while it was slightly stronger in the RICO clouds. In general, the LWC in stratocumulus remains close to adiabatic up to cloud top (Brenguier et al., 2003; Pawlowska and Brenguier, 2003), while it is significantly diluted in the RICO cumulus clouds. Cloud sampled during RICO show indeed that peak LWC values decrease continuously with height down to about 50% of the adiabatic value 1 km above cloud base, while median LWC values drop down to about 30% of the adiabatic within the first 200 m.

Droplet spectra were sampled at 1 Hz (a flight distance of about 100 m). Cloudy samples are defined as samples with a LWC greater than 0.025 g m$^{-3}$ and a cloud droplet number concentration $N_c$ greater than 5 cm$^{-3}$. Figure 1 shows a scatter-plot of the droplet number concentration (M0) and the LWC ($\propto$M3), with different colours for the ACE2 (blue) and the RICO (red) data sets. The number concentrations are lower in RICO, but the LWC values are similar in both data sets, up to 2 g m$^{-3}$. Overall, the two campaigns provide a set of 27 623 cloud droplet spectra in total: 19 151 from 8 ACE-2 cases (fr9720, fr9721, fr9728, fr9730, fr9731, fr9733, fr9734, fr9735) and 8472 from 7 RICO cases (RF06, RF07, RF08, RF09, RF11, RF12, RF13), sampled at various levels from the cloud base to the top. Both data sets have first been analyzed separately to derive tuning parameter values specific to the stratocumulus and cumulus regimes. Interestingly, the conclusions are very similar and the analysis is presented here with both data sets merged.

17643

## 6 From the small scale to the cloud system scale

In this exercise, the spatial scale is an important issue. Indeed, airborne cloud particle spectrometers have a limited sampling section, so that a very tiny fraction of air is sampled along the flight track. For instance, the Fast-FSSP has a sampling section of 0.1 mm$^2$. Droplet counts are therefore cumulated over 100 m for the measured distribution to become statistically significant (about 1000 droplets sampled at a number concentration of 100 cm$^{-3}$). For drizzle and precipitation drops, the number concentration decreases exponentially with size, but the sampling section of the drizzle and precipitation particle spectrometers does not increase accordingly. One is thus tempted to increase the sample length, hence increase the number of sampled particles, to better characterize a spectrum. Droplet spectra, however, are highly variable at scales smaller than 100 m (Pawlowska et al., 1997). This spatial variability raises two important issues when averaging spectra over long distances for characterizing cloud system representative properties.

First, the spatial variability is linearly smoothed out when cumulating particle counts over a long sample and this may become an issue if the physical process of interest is highly non-linear. Although they are second order, the biases arising from using non-linear combinations of linearly averaged microphysical parameters may thus occasionally lead to flawed conclusions. A typical example is when characterizing the spectral width for studies of the collection process. Indeed, the droplet collection (collision and coalescence) is highly sensitive to the presence of both small and large droplets in the same micro-volume of cloudy air. Thus it depends non-linearly on the width of the droplet spectrum. In cumulus clouds for instance, narrow droplet spectra are observed at all levels, but their mode increases from cloud base to the top. If droplet measurements are cumulated over flight legs ascending from the cloud base to the top, the resulting spectrum might thus be much broader than locally, hence suggesting enhanced collection, while droplets located at different levels have no chance to collide and coalesce. It is therefore recommended to cumulate droplet counts only

17644

on flight legs that are statistically homogeneous in term of spectral properties.

The second issue arises when averaging CDSD intensive properties, such as the radius of the $p^{th}$ moment instead of extensive[1] properties such as the moment itself. For instance the light extinction in a cloud depends on the second moment, as $\sigma_{ext}=\pi Q_{ext} M_2=\pi Q_{ext} Nr_2^2$, where $r_2$, is the mean radius of the 2nd moment or mean surface radius of the droplet spectrum. The mean extinction in a cloud layer, is therefore equal to $\langle\sigma_{ext}\rangle =\pi Q_{ext} \langle M_2\rangle$, which is different from $\pi Q_{ext} \langle N\rangle \langle r_2\rangle^2$. The latter formulation, however, is the most frequently used because observational data sets are often processed to derive the mean droplet number concentration and the mean surface radius, or effective radius, instead of the mean second moment of the size distributions. Diluted cloud volumes often show intensive properties that are quite different from the ones observed in undiluted volumes because of the impact of entrainment and mixing processes (Burnet and Brenguier, 2007). However, when using the second formulation, diluted volumes are given the same weight as the undiluted ones, while they very little contribute to the mean value of the corresponding moment.

In general, one shall therefore avoid averaging spectral properties such as any mean radius of the distribution or ratio of such variables as the $k$ coefficient in Martin et al. (1994) that do not depend on the droplet concentration, hence might overemphasize the contributions of highly diluted cloud volumes. The tuning of the parametric functions described hereafter is thus based on moments of the size distribution instead of mean radii of the moments, and 4 moments ($M_1$, $M_2$, $M_5$ and $M_6$) are considered separately.

---

[1] "intensive" and "extensive" are defined here with regards to the number of particles, instead of number concentration or mixing ratio.

17645

## 7 Tuning of the parametric functions

### 7.1 Constant tuning parameter

Figure 2 summarizes the analysis. The first three rows show scatter-plots of the tuning parameter values for the four moments, from left to right. The range of variation of the moment values has been divided in 10 classes on a Log scale. The first row is for the Lognormal parametric function, the second one for the Generalized Gamma with $\alpha=1$ (GG1), and the third one for the Generalized Gamma with $\alpha=3$ (GG3). The last row shows the number of samples in each moment class.

Each grey point represents the value of the tuning parameter that best fits the specified moment of an observed spectrum. Superimposed to the scatter-plot, two thin lines represent the 25th and 75th percentiles of the tuning parameter values in each moment class. The circles and triangles are the tuning parameter values that minimize, in each moment class, the arithmetic and the geometric standard deviation of the absolute and relative errors, respectively. On top of each graph, the number in brackets on the left (right) hand side is the tuning parameter value that minimizes the absolute (relative) error over the whole range of variation of the specified moment.

For the Lognormal distribution, the top row suggests that a $\sigma_g$ value between 1.3 and 1.4 provides accurate estimations, for the moment values that are the most frequently observed, i.e. $10^3\,\mu\mathrm{m}\,\mathrm{cm}^{-3}$ for $M_1$, $5.10^3\,\mu\mathrm{m}^2\,\mathrm{cm}^{-3}$ for $M_2$, from $10^6$ to $2.10^7\,\mu\mathrm{m}^5\,\mathrm{cm}^{-3}$ for $M_5$ and from $10^7$ to $2.10^8\,\mu\mathrm{m}^6\,\mathrm{cm}^{-3}$ for $M_6$. For $M_1$ and $M_2$, however, this value underestimates the optimum $\sigma_g$ value at small moment values, hence overestimates the small moment values, and inversely for the large moment values. For the higher moments, $M_5$ and $M_6$, the optimum $\sigma_g$ value does not vary significantly with the value of the moment. The sensitivity test to the radius threshold value that separates droplets from drops in the bulk scheme reveals that these two higher moments are more sensitive than the lower ones, although the impact, even with a threshold value of $27.5\,\mu$m, is hardly noticeable. This $\sigma_g$ value is close to the revised value that was recommended in the 9th inter-comparison exercise of the GCSS BLWG ($\sigma_g=1.2$) for the parameteri-

17646

zation of cloud droplet sedimentation (Ackerman et al., 2008).

For the Generalised Gamma distribution, the results are similar, with optimum values of the tuning parameter $\nu$ of the order of 10 for GG1 and slightly larger than 1 for GG3, although the trends are reversed compared to the Lognormal since increasing values of the $\nu$ parameters correspond to narrower spectra. A value of $\nu_3$ equal to 1 corresponds in the formulation of the auto-conversion in Seifert and Beheng (2006, Eq. 4) to a $\nu_c$ value equal to 0, which is commonly used.

This set of scatter-plots suggests that there is no single parameter value that minimizes both errors for the 4 moments concomitantly. The optimum value indeed depends on the application and one might select a $M_1$ optimum value for the prognostic of peak supersaturation in a CCN activation scheme, a $M_2$ specific one for radiative transfer and the sedimentation flux of particle number concentration, a $M_5$ specific one for the sedimentation flux of particle water content, and a $M_6$ specific one for the retrieval of cloud properties from a radar reflectivity.

It might be questionable, and less practicable, to use different values of the tuning parameter for the analytical function that describes the droplet distribution in a numerical model, although this is a common practice when using in a numerical model parameterizations of diverse origins, hence relying on different values of the tuning parameter or even different parametric functions. For instance the bulk microphysical schemes tested by the GCSS boundary layer working group are based on a Lognormal function for parameterization of droplet sedimentation (Ackerman et al., 2008), whereas the autoconversion scheme often relies on different hypotheses. Some authors use different distribution hypotheses in the same process parameterization (see Table 1 in Gilmore and Straka, 2008). For better consistency, we propose a compromise that partly satisfies all types of applications. A trade-off value of the tuning parameter is derived as:

$$p^* = \frac{1}{8n} \sum_{i,j,k} n_{i,j} p_{i,j,k}, \qquad (9)$$

where $n$ is the total number of cloud samples, $i \in [1:10]$ stand for the moment class,

$j \in [1,2,5,6]$ stands for the moment, and $k \in [1,2]$, corresponds to either the absolute or relative error. $n_{i,j}$, is the number of samples in class $i$ of the moment $M_j$ and $p_{i,j,k}$, is the optimum tuning parameter value in the class $i$ of the moment $j$, for the absolute and relative errors, respectively.

This trade-off value of the tuning parameter, $\sigma_g^*=1.34$ for the Lognormal, $\nu_1^*=10.3$ for GG1 and $\nu_3^*=1.11$ for GG3, is represented in Fig. 2 by a horizontal bar and it is reported in Table 2, with the resulting offset and standard deviations of the absolute and relative errors.

Figure 3 shows scatter-plots of the absolute errors in each moment class, as in Fig. 2, for the Lognormal (first row), the GG1 (second row) and the GG3 (third row) parametric functions. The grey points represent the error for each sampled spectrum, the thin lines denote the 25th and the 75th percentiles of the absolute error distribution in each class, and the circle and error bars indicate the arithmetic mean (offset) and standard deviation of the absolute error values in each class. Note that for practical reasons, the error values are normalized in each graph, as specified in the figure caption. Figure 4 is similar for the relative errors, although errors are not normalized in this case. These figures confirm that a single parameter value provides accurate descriptions of the droplet spectra in the most common range of moment values, but significantly deviates at low moment values for the relative error and high moment values for both errors, although such samples are less frequently observed.

## 7.2 Variable tuning parameter

In a second step, we explore the potential of diagnosing the tuning parameter, using the prognostic variables of a bulk parameterization, i.e. $N$ or $q_c$. The tuning parameter shows the greatest sensitivity to the LWC. This is illustrated in Fig. 5 that is similar to Fig. 2, except that the x-axis now represents the LWC.

The optimum parameter values, in each $q_c$ class (10 classes) of each moment (4 moments) and for both the absolute (circles) and relative (triangles) errors, are combined and the function of $q_c$ that best fits the 80 values is derived for the Lognormal, the GG1

and the GG3 successively, leading to the following parameterizations:

$$\sigma_g^p = -0.056 \cdot \ln(q_c) + 1.24, \tag{10}$$

$$v_1^p = 14.5 \cdot q_c + 6.7, \tag{11}$$

$$v_3^p = 1.58 \cdot q_c + 0.72, \tag{12}$$

where $q_c$ is expressed in $g\,m^{-3}$. They are represented in each graph of Fig. 5 by a thick line.

Figures 6 and 7, similar to Figs. 3 and 4 show the improvement on the absolute and relative errors, respectively, in each moment class. The offsets and standard deviations of the absolute and relative errors over the whole range of moment values are summarized in Table 3.

The comparison with Table 2, attests that both the absolute and relative errors have been reduced in term of offset and standard deviation, although the main improvement is for the absolute error at large values of the moments (Figs. 3 and 6), and for the relative error at both small and large values of the moments (Figs. 4 and 7).

## 8  Summary and conclusions

Droplet spectra measured in stratocumulus and shallow cumulus clouds have been examined to fit three parametric functions, i.e. the Lognormal, and the Generalized Gamma functions with $\alpha$=1 and $\alpha$=3, successively, that are frequently used in bulk parameterizations of the microphysics to represent droplet size distributions.

These functions have three independent parameters. Two are constrained by the values of the droplet number concentration and liquid water content. An optimum value of the third parameter, $\sigma_g$ for the Lognormal, $v_1$ for the GG1 and $v_3$ for the GG3, has been derived for each measured spectrum, that minimizes the difference between the observed spectrum and the parametric function. The difference has been measured

17649

using integral properties of the droplet spectra, namely 4 moments of the size distribution, $M_1$ that is used in CCN activation schemes, $M_2$ in radiative transfer calculations and droplet sedimentation parameterization, $M_5$ for parameterization of droplet sedimentation, and $M_6$ for radar reflectivity calculations.

The range of variation of each moment has been divided in 10 classes on a Logscale and the arithmetic and geometric means of the optimum parameter values have been calculated in each class. The absolute and relative errors have similarly been quantified in each class, and over the whole range of variation of each moment. As expected, the optimum parameter values however are slightly different depending on which integral property is used for the minimization. A trade-off parameter value has then been proposed, that minimizes both the absolute and the relative errors on the 4 moments of the distributions.

In a second step, parameterizations are proposed where the optimum parameter value depends on the LWC, and the absolute and relative errors have been quantified for each moment separately. Such a varying tuning parameter slightly improves both the absolute and relative errors for the moment values that are the most frequently observed, and it significantly improves the error at the lowest and largest values of the moments.

The potential of using the third parameter as a prognostic variable in a bulk scheme has been explored, but because of the large variability of spectral shapes and the diversity of physical processes that are responsible for this variability, condensational growth, mixing and evaporation, droplet scavenging, and collection, we have not been able to isolate one process that could be considered as the most determinant. Further analysis or numerical simulations with bin microphysical schemes might help at solving the issue. However, considering the limitations inherent to the bulk approach, one might also conclude that the accuracy of the parameterizations proposed here is sufficient for most of the topics that can be addressed with a bulk scheme.

17650

## References

5   Ackerman, A. S., van Zanten, M. C., Stevens, B., Savic-Jovcic, V., Bretherton, C. S., Chlond, A., Gloaz, J.-G., Jiang, H., Khairoutdinov, M., Krueger, S. K., Lewellen, D. C., Lock, A., Moeng, C.-H., Nakamura, K., Petters, M. D., Snider, J. R., Weinbrecht, S., and Zulauf, M.: Large-eddy simulations of a drizzling, stratocumulus-topped marine boundary layer, Mon. Weather Rev., 137, 1083–1110, 2008.

10   Atlas, D.: The estimation of cloud parameters by radar, J. Meteorol., 11, 309–317, 1954.

Berry, E. X. and Reinhardt, R. L.: An analysis of cloud drop growth by collection Part II. Single initial distributions, J. Atmos. Sci., 31, 1825–1831, 1974.

Brenguier, J.-L., Bourrianne, T., de Araujo Coelho, A., Isbert, R. J., Peytavi, R., Trevarin, D., and Weschler, P.: Improvements of droplet distribution size measurements with the fast-FSSP

15   (forward scattering spectrometer probe), J. Atmos. Ocean. Tech., 15, 1077–1090, 1998.

Brenguier, J.-L., Pawlowska, H., Schüller, L., Preusker, R., Fischer, J., and Fouquart, Y.: Radiative properties of boundary layer clouds: droplet effective radius versus number concentration, J. Atmos. Sci., 57, 803–821, 2000.

Brenguier, J.-L., Pawlowska, H., and Schüller, L. J.: Cloud microphysical and radiative proper-

20   ties for parameterization and satellite monitoring of the indirect effect of aerosol on climate, J. Geophys. Res., 108, 8632, doi:10.1029/2002JD002682, 2003.

Burnet, F. and Brenguier, J.-L.: Observational study of the entrainment-mixing process in warm convective clouds, J. Atmos. Sci., 64, 1995–2011, 2007.

Clark, T. L.: Use of log-normal distributions for numerical calculation of condensation and col-

25   lection, J. Atmos. Sci., 33, 810–821, 1976.

Cohard, J.-M. and Pinty, J.-P.: A comprehensive warm microphysical bulk scheme, part I: Description and selective tests, Q. J. Roy. Meteor. Soc., 126, 1815–1842, 2000.

Feingold, G. and Levin, Z.: The lognormal fit to raindrop spectra from frontal convective clouds in Israel, J. Clim. Appl. Meteorol., 25, 1346–1363, 1986.

Gilmore, M. S. and Straka, J. M.: The Berry and Reinhardt autoconversion : A digest. J. Appl. Meteorol., 47, 375–396, 2008.

Hansen, J. E. and Travis, L. D.: Light scattering in planetary atmospheres, Space Sci. Rev., 16, 527–610, 1974.

5   Kessler, E.: On the Distribution and Continuity of Water Substance in Atmospheric Circulations, Meteor. Monogr., 32, Amer. Meteor. Soc., 84 pp., 1969.

Khairoutdinov, M. and Kogan, Y.: A new cloud physics parameterization in a large-eddy simulation model of marine stratocumulus, Mon. Weather Rev., 128, 229–243, 2000.

Kogan, Y.: The simulation of a convective cloud in a 3-D model with explicit microphysics. Part

10   I: Model description and sensitivity experiments, J. Atmos. Sci., 48, 1160–1189, 1991.

Martin, G. M., Johnson, D. W., and Spice, A.: The measurement and parameterization of effective radius of droplets in warm stratocumulus clouds, J. Atmos. Sci., 51, 1823–1842, 1994.

Liu, Y. and Hallett, J.: On size distributions of cloud droplets growing by condensation: A new

15   conceptual model, J. Atmos. Sci., 55, 527–536, 1998.

Liu, Y. and Daum, P. H.: Spectral dispersion of cloud droplet size distributions and the parameterization of cloud droplet effective radius, Geophys. Res. Lett., 27, 1903–1906, 2000.

Liu, Y. and Daum, P. H.: Parameterization of the autoconversion process. Part I: Analytical formulation of the Kessler-type parameterizations, J. Atmos. Sci., 61, 1539–1548, 2004.

20   Manton, M. J. and Cotton, W. R.: Formulation of approximate equations for modeling moist deep convection on the mesoscale, Atmos. Sci., 266, Dept. of Atmos. Sci., Colorado State University, 1977.

Milbrandt, J. A. and Yau, M. K.: A multimoment bulk microphysics parameterization. Part II: A proposed three-moment closure and scheme description, J. Atmos. Sci., 62, 3065–3081,

25   2005.

Pawlowska, H., Brenguier, J.-L., and Salut, G.: Optimal non-linear estimation for cloud particle measurements, J. Atmos. Ocean. Tech., 14, 88–104, 1997.

Pawlowska, H. and Brenguier, J.-L.: An observational study of drizzle formation in stratocumulus clouds for general circulation model (GCM) parameterizations, J. Geophys. Res.,

30   108(D15), 8630, doi:10.1029/2002JD002679, 2003.

Rogers, R. R. and Yau, M. K.: A Short Course in Cloud Physics, Third edition, International Series in Natural Philosophy, Pergammon Press, 293 pp., 1989.

Rauber, R. M., Stevens, B., Ochs, H. T., Knight, C., Albrecht, B. A., Blyth, A. M., Fairall, C. W.,

Jensen, J. B., Lasher-Trapp, S. G., Mayol-Bracero, O. L., Vali, G., Anderson, J. R., Baker, B. A., Bandy, A. R., Burnet, F., Brenguier, J.-L., Brewer, W. A., Brown, P. R. A., Chuang, P., Cotton, W. R., Di Girolamo, L., Geerts, B., Gerber, H., Göke, S., Gomes, L., Heikes, B. G., Hudson, J. G., Kollias, P., Lawson, R. P., Krueger, S. K., Lenschow, D. H., Nuijens, L., O'Sullivan, D. W., Rilling, R. A., Rogers, D. C., Siebesma, A. P., Snodgrass, E., Stith, J. L., Thornton, D. C., Tucker, S., Twohy, C. H., and Zuidema, P.: Rain in shallow cumulus over the ocean: The RICO campaign, B. Am. Meteorol. Soc., 88, 1912–1928, 2007.

Seifert, A. and Beheng, K. D.: A double-moment parameterization for simulating autoconversion, accretion and self-collection, Atmos. Res, 59–60, 265–281, 2001.

Seifert, A. and Beheng, K. D.: A two-moment cloud microphysics parameterization for mixed-phase clouds. Part 1: Model description, Meteorol. Atmos. Phys., 92, 45–66, 2006.

Tripoli, G. J. and Cotton, W. R.: A numerical investigation of several factors contributing to the observed variable intensity of deep convection over South Florida, J. Atmos. Sci., 19, 1037–1063, 1980.

Twomey, S.: The nuclei of natural cloud formation. Part II: The supersaturation in natural clouds and the variation of cloud droplet concentration, Geofys. Pura. Appl., 43, 243–249, 1959.

Warner, J.: The microstructure of cumulus clouds. Part I. General features of the droplet spectrum, J. Atmos. Sci., 26, 1049–1059, 1969a.

Warner, J.: The microstructure of cumulus clouds. Part II. The effect on droplet size distribution of cloud nucleus spectrum and updraft velocity, J. Atmos. Sci., 26, 1272–1282, 1969b.

Warner, J.: The microstructure of cumulus clouds. Part III. The nature of the updraft, J. Atmos. Sci., 27, 682–688, 1970.

Warner, J.: The microstructure of cumulus clouds. Part IV. The effect on the droplet spectrum of mixing between cloud and environment, J. Atmos. Sci., 30, 256–261, 1973a.

Warner, J.: The microstructure of cumulus clouds. Part V. Changes in droplet size distribution with cloud age, J. Atmos. Sci., 30, 1724–1726, 1973b.

Williams, R. and Wojtowicz, P. J.: A Simple Model for Droplet Size Distribution in Atmospheric Clouds, J. Appl. Meteorol., 21, 1042–1044, 1982.

Ziegler, C. L.: Retrieval of thermal and microphysical variables in observed convective storms. Part I: Model development and preliminary testing, J. Atmos. Sci., 42, 1487–1509, 1985.

17653

**Table 1.** Typical bulk parameterizations using two particle categories with, from left to right, the value of the threshold radius between the two categories, the number of independent variables for the description of the droplet size distribution (CDSD), the parameterized microphysical processes, the methodology adopted for the development of the parametrization, and the CDSD parametric representation.

| Reference | Separation radius $r_0$ | Number of independent variables for the description of the CDSD | Microphysical processes | Methodology& CDSD hypothesis |
|---|---|---|---|---|
| Kessler (1969) | NA | $q_c$ | autoconversion | Empirical CDSD: monodispersed |
| Manton and Cotton (1977) | NA | $q_c, N_c$ | autoconversion | Analytical CDSD: monodispersed |
| Berry and Reinhardt (1974) | variable, $\sim 41\,\mu m$ | $q_c, N_c, \sigma_x$ | autoconversion | Empirical, $\sim 30$ spectra from 0-D bin simulations, CDSD: GG3 |
| Khairoutdinov and Kogan (2000) | $25\,\mu m$ | $q_c, N_c$ | autoconversion | Empirical, 100 000 spectra from 3-D bin simulations of Sc, CDSD: GG1 |
| Liu and Daum (2004) | NA | $q_c, N_c, d$ | autoconversion | Analytical, CDSD: GG1 |
| Seifert and Beheng (2001, 2006) | $41\,\mu m$ | $q_c, N_c,$ $v_c = v_3 - 1$ | autoconversion | Analytical and empirical, GG3 and spectra from 1-D bin simulations, CDSD: GG3 |
| Cohard and Pinty (2000) | NA | $q_c, N_{CCN}$ | activation | Analytical CDSD: GG3 |
| Ackerman (2008) | NA | $q_c, N_c, \sigma_g$ | Cloud droplet sedimentation | Analytical CDSD: Lognormal |

17654

**Table 2.** Values of the arithmetic mean $\mu_{abs}$ and the arithmetic standard deviation $\sigma_{abs}$ of the absolute errors and of the geometric mean $\mu_{rel}$ and the geometric standard deviation $\sigma_{rel}$ of the relative errors calculated for $M_1$, $M_2$, $M_5$, $M_6$, for the Lognormal, the GG1 and the GG3 parametric functions, when using the constant trade-off tuning parameters values, $\sigma_g^*$ for the Lognormal, $\nu_1^*$ for the GG1 and $\nu_3^*$ for the GG3.

| | $M_1$ | $M_2$ | $M_5$ | $M_6$ |
|---|---|---|---|---|
| Lognormal, $\sigma_g^*=1.34$ | | $\mu_{abs}\pm\sigma_{abs}$ | | |
| | $-0.82\pm31.1$ | $-40\pm266$ | $7.9\pm30.3$ | $23.7\pm103.1$ |
| | $(\mu m\,cm^{-3})$ | $(\mu m^2\,cm^{-3})$ | $(10^5\,\mu m^5\,cm^{-3})$ | $(10^6\,\mu m^6\,cm^{-3})$ |
| | | $\mu_{rel}\,{}_/^\times\,\sigma_{rel}$ | | |
| | $1.001\,{}_/^\times\,1.054$ | $1.004\,{}_/^\times\,1.052$ | $0.972\,{}_/^\times\,1.332$ | $0.910\,{}_/^\times\,1.751$ |
| Generalized Gamma, $\alpha=1,\ \nu_1^*=10.3$ | | $\mu_{abs}\pm\sigma_{abs}$ | | |
| | $-5.3\pm32.2$ | $-62\pm274$ | $6.5\pm28.9$ | $16.9\pm93.2$ |
| | $(\mu m\,cm^{-3})$ | $(\mu m^2\,cm^{-3})$ | $(10^5\,\mu m^5\,cm^{-3})$ | $(10^6\,\mu m^6\,cm^{-3})$ |
| | | $\mu_{rel}\,{}_/^\times\,\sigma_{rel}$ | | |
| | $1.002\,{}_/^\times\,1.054$ | $1.000\,{}_/^\times\,1.052$ | $0.958\,{}_/^\times\,1.332$ | $0.870\,{}_/^\times\,1.751$ |
| Generalized Gamma, $\alpha=3,\ \nu_3^*=1.11$ | | $\mu_{abs}\pm\sigma_{abs}$ | | |
| | $-12.0\pm34.4$ | $-84\pm282$ | $3.4\pm25.8$ | $5.1\pm77.9$ |
| | $(\mu m\,cm^{-3})$ | $(\mu m^2\,cm^{-3})$ | $(10^5\,\mu m^5\,cm^{-3})$ | $(10^6\,\mu m^6\,cm^{-3})$ |
| | | $\mu_{rel}\,{}_/^\times\,\sigma_{rel}$ | | |
| | $0.991\,{}_/^\times\,1.054$ | $0.996\,{}_/^\times\,1.052$ | $0.926\,{}_/^\times\,1.332$ | $0.803\,{}_/^\times\,1.751$ |

17655

**Table 3.** Same as Table 2 when using the variable tuning parameter parameterizations, $\sigma_g^p$ for the Lognormal, $\nu_1^p$ for the GG1 and $\nu_3^p$ for the GG3.

| | $M_1$ | $M_2$ | $M_5$ | $M_6$ |
|---|---|---|---|---|
| Lognormal, $\sigma_g^p$ | | $\mu_{abs}\pm\sigma_{abs}$ | | |
| | $4.3\pm28.9$ | $23\pm227$ | $0.2\pm18.2$ | $1.2\pm54.2$ |
| | $(\mu m\,cm^{-3})$ | $(\mu m^2\,cm^{-3})$ | $(10^5\,\mu m^5\,cm^{-3})$ | $(10^6\,\mu m^6\,cm^{-3})$ |
| | | $\mu_{rel}\,{}_/^\times\,\sigma_{rel}$ | | |
| | $1.007\,{}_/^\times\,1.052$ | $1.003\,{}_/^\times\,1.050$ | $0.978\,{}_/^\times\,1.292$ | $0.918\,{}_/^\times\,1.651$ |
| Generalized Gamma, $\alpha=1,\ \nu_1^p$ | | $\mu_{abs}\pm\sigma_{abs}$ | | |
| | $-2.3\pm29.0$ | $-17\pm226$ | $0.3\pm18.1$ | $-1.4\pm53.5$ |
| | $(\mu m\,cm^{-3})$ | $(\mu m^2\,cm^{-3})$ | $(10^5\,\mu m^5\,cm^{-3})$ | $(10^6\,\mu m^6\,cm^{-3})$ |
| | | $\mu_{rel}\,{}_/^\times\,\sigma_{rel}$ | | |
| | $0.997\,{}_/^\times\,1.053$ | $0.996\,{}_/^\times\,1.050$ | $0.973\,{}_/^\times\,1.300$ | $0.893\,{}_/^\times\,1.672$ |
| Generalized Gamma, $\alpha=3,\ \nu_3^p$ | | $\mu_{abs}\pm\sigma_{abs}$ | | |
| | $-8.6\pm29.9$ | $-37\pm226$ | $-1.7\pm18.0$ | $-8.9\pm52.7$ |
| | $(\mu m\,cm^{-3})$ | $(\mu m^2\,cm^{-3})$ | $(10^5\,\mu m^5\,cm^{-3})$ | $(10^6\,\mu m^6\,cm^{-3})$ |
| | | $\mu_{rel}\,{}_/^\times\,\sigma_{rel}$ | | |
| | $0.984\,{}_/^\times\,1.052$ | $0.990\,{}_/^\times\,1.050$ | $0.943\,{}_/^\times\,1.303$ | $0.826\,{}_/^\times\,1.682$ |
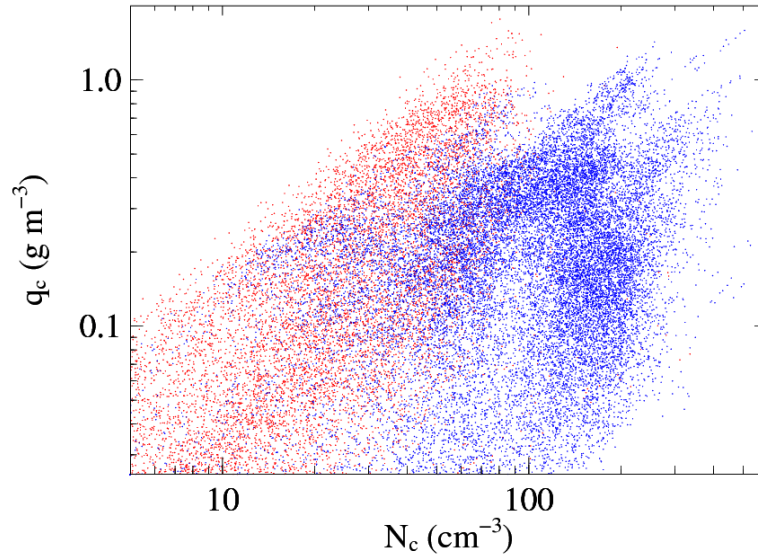
**Fig. 1.** Scatter-plot of the droplet number concentration, $N_c$, and the LWC, $q_c$, for droplet spectra sampled at 1 Hz, during the ACE2 (blue) and RICO (red) field experiments.
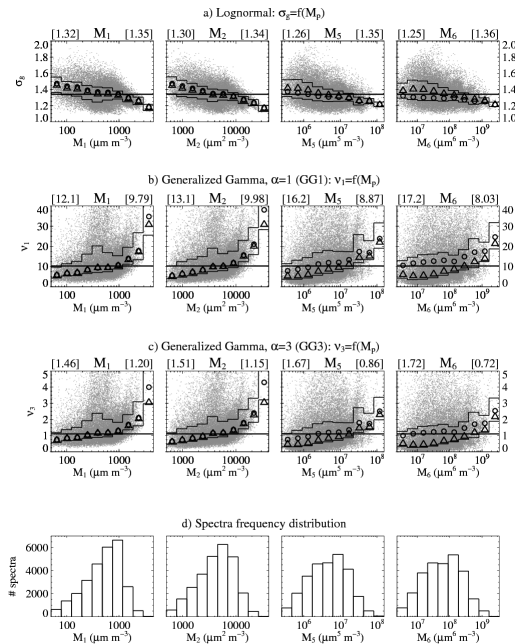
17657



**Fig. 2.** Scatter-plots (grey points) of the tuning parameter values as a function, from left to right, of the $M_1$, $M_2$, $M_5$, and $M_6$ moment values. The x-axis is divided in 10 classes on a Logscale. The thin lines denote the 25th and the 75th percentiles of the tuning parameter distribution in each class. The circles and triangles denote the tuning parameter value that minimizes the standard deviation of the absolute error and the geometric standard deviation of the relative error in each class, respectively. The horizontal thick line denotes the constant trade-off value of the tuning parameter. The top row is for the Lognormal function, the second and third rows are for the Generalized Gamma functions with $\alpha$=1 and $\alpha$=3, respectively. On top of each graph, the number in brackets on the left (right) hand side is the tuning parameter value that minimizes the absolute (relative) error over the whole range of variation of the specified moment. The fourth row shows the number of sampled spectra in each moment class.
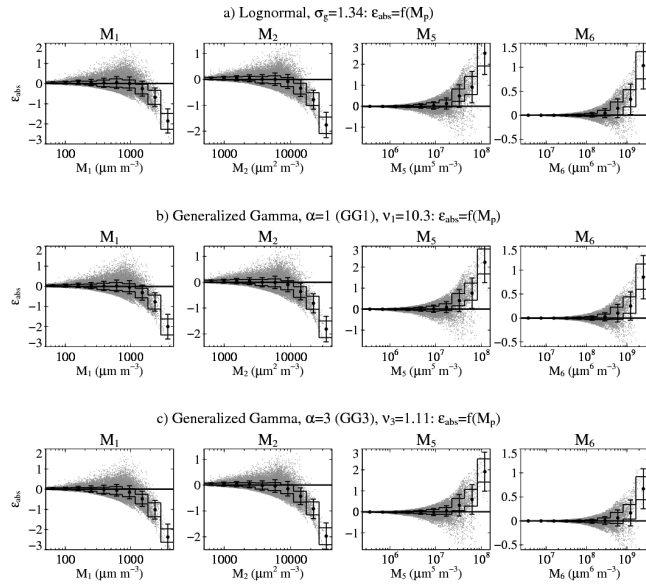
17658

a) Lognormal, $\sigma_g$=1.34: $\varepsilon_{abs}$=f($M_p$)

b) Generalized Gamma, $\alpha$=1 (GG1), $\nu_1$=10.3: $\varepsilon_{abs}$=f($M_p$)

c) Generalized Gamma, $\alpha$=3 (GG3), $\nu_3$=1.11: $\varepsilon_{abs}$=f($M_p$)

**Fig. 3.** Scatter-plots (grey points) of the absolute errors between the observed spectrum moment value and the one of the parametric function using the trade-off value of the tuning parameter $\sigma_g^*$=1.34 for the Lognormal function (top row), $\nu_1^*$=10.3 for GG1 (2nd row), and $\nu_3^*$=1.11 for GG3 (3rd row), as a function of the moment values. The X-axis is divided in 10 classes as in Fig. 2. The thin lines denote the 25th and the 75th percentiles of the absolute error distribution in each class. The circles and the error bars denote the arithmetic mean and the arithmetic standard deviation of the absolute error values in each class. The absolute errors are normalized from left to right respectively by 100 $\mu$m cm$^{-3}$ for $M_1$, 1000 $\mu$m$^2$ cm$^{-3}$ for $M_2$, 10$^7$ $\mu$m$^5$ cm$^{-3}$ for $M_5$ and 10$^9$ $\mu$m$^6$ cm$^{-3}$ for $M_6$.

17659

a) Lognormal, $\sigma_g$=1.34: $\varepsilon_{rel}$=f($M_p$)

b) Generalized Gamma, $\alpha$=1 (GG1), $\nu_1$=10.3: $\varepsilon_{rel}$=f($M_p$)

c) Generalized Gamma, $\alpha$=3 (GG3), $\nu_3$=1.11: $\varepsilon_{rel}$=f($M_p$)
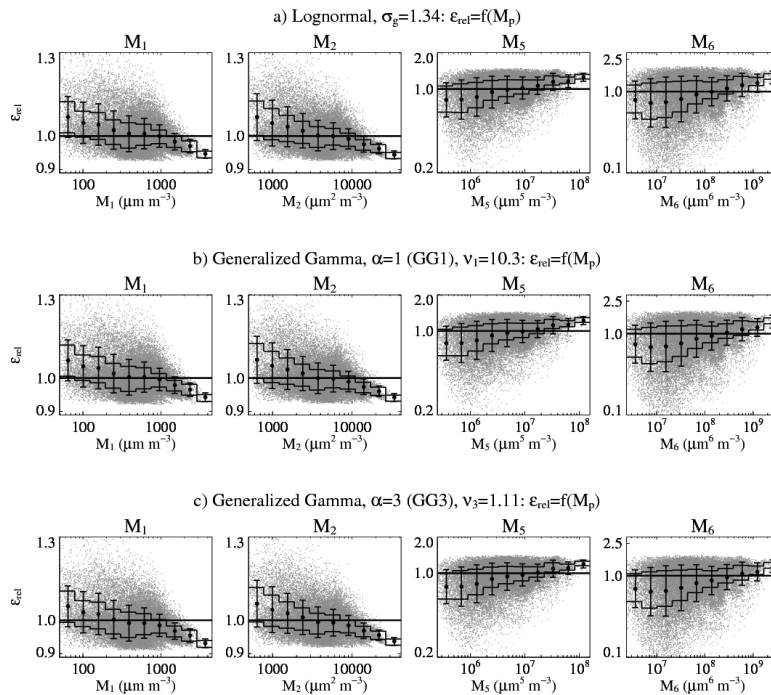
**Fig. 4.** Same as Fig. 3 for the relative errors. The circles and the error bars denote the geometric mean and the geometric standard deviation of the relative error value distribution in each moment class. The relative errors are not normalized.
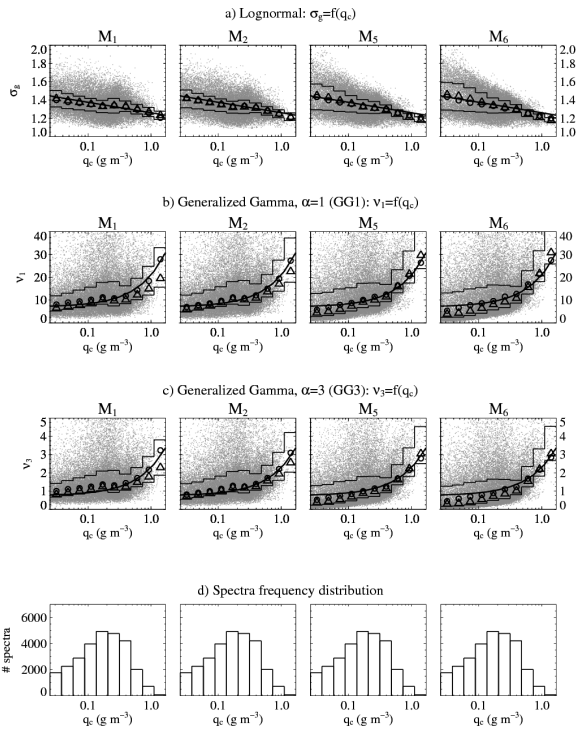
17660

**Fig. 5.** Same as Fig. 2 but plotted as a function of the LWC, $q_c$. The thick line represents the proposed parameterizations for the variable tuning parameter.

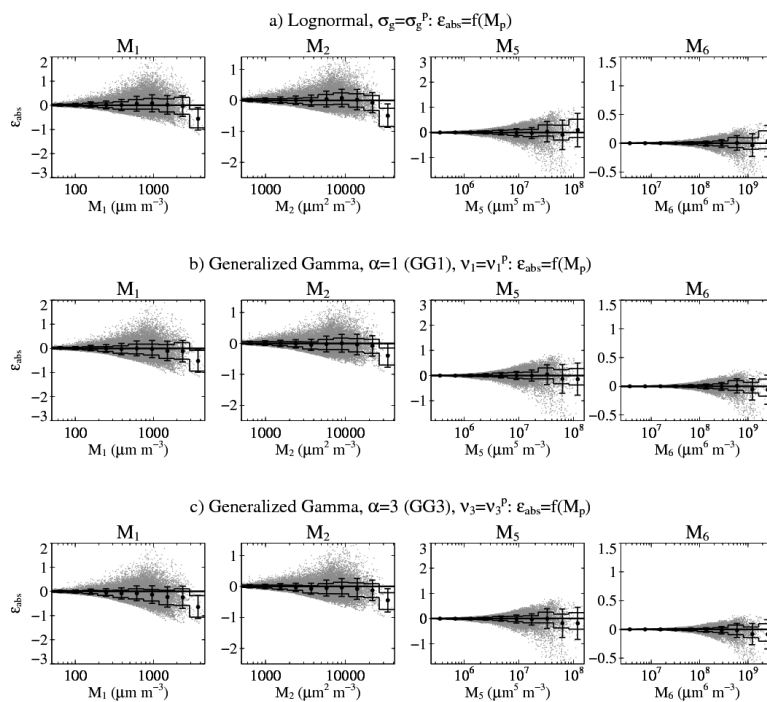**Fig. 6.** Same as Fig. 3 using the proposed parameterization for the variable tuning parameter.

a) Lognormal, $\sigma_g = \sigma_g^p$: $\varepsilon_{rel} = f(M_p)$

b) Generalized Gamma, $\alpha = 1$ (GG1), $\nu_1 = \nu_1^p$: $\varepsilon_{rel} = f(M_p)$

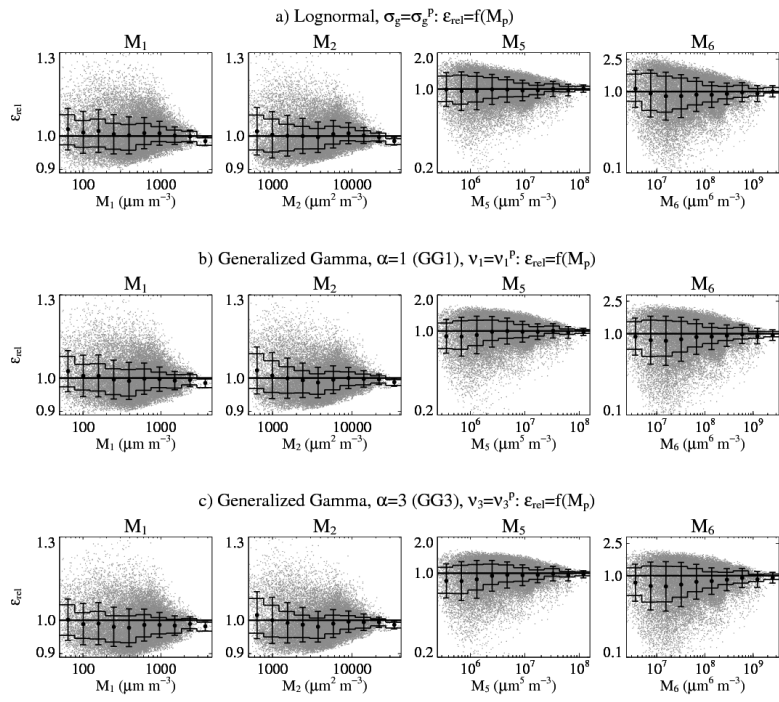c) Generalized Gamma, $\alpha = 3$ (GG3), $\nu_3 = \nu_3^p$: $\varepsilon_{rel} = f(M_p)$

**Fig. 7.** Same as Fig. 4 using the proposed parameterization for the variable tuning parameter.

17663